DOI: 10.1177/0003702820920652

Paper type: Special Issue: Microplastics Submitted Paper

Microplastics Differ Between Indoor and Outdoor Air Masses: Insights from Multiple Microscopy Methodologies

Emily Gaston,[1,*] Mary Woo,[1] Clare Steele,[1] Suja Sukumaran,[2] Sean Anderson[3]

[1]California State University Channel Islands, Environmental Science and Resource Management Program, CA 93012 USA

[2]Thermo Fisher Scientific, San Jose, CA 95134 USA

[3]California State University Channel Islands, Environmental Science and Resource Management Program, PIRatE Lab, CA, 93012 USA

*Corresponding author email: Emily.Gaston@csuci.edu

Abstract

The abundance and distribution of microplastic (<5 mm) has become a growing concern, particularly over the past decade. Research to date has focused on water, soil, and organism matrices but generally disregarded air. We explored airborne microplastic inside and outside of buildings in coastal California by filtering known volumes of air through glass fiber filters, which were then subsequently characterized with a variety of microscopy techniques: gross traditional microscopy, fluorescent microscopy following staining with Nile red, micro-Raman spectroscopy, and micro-Fourier transform infrared (FT-IR) spectroscopy. Microplastics permeated the air, with indoor (3.3±2.9 fibers and 12.6±8.0 fragments m^{-3}; mean±1 SD) harboring twice as much as outdoor air (0.6 ±0.6 fibers and 5.6±3.2 fragments m^{-3}). Microplastic fiber length did not differ significantly between indoor and outdoor air, but indoor microplastic fragments (58.6±55 µm) were half the size of outdoor fragments (104.8±64.9 µm). Micro-Raman and FT-IR painted slightly different pictures of airborne plastic compounds, with micro-Raman suggesting polyvinyl chloride dominates indoor air, followed by polyethylene (PE) and micro-FT-IR showing polystyrene dominates followed by PE and polyethylene terephthalate. The ubiquity of airborne microplastic points to significant new potential sources of plastic inputs to terrestrial and marine ecosystems and raises significant concerns about inhalation exposure to humans both indoors and out.

DOI: 10.1177/0003702820920652

Keywords: Pollution, polymer, waste, inhalation, ecotoxicology, air quality, microspectroscopy, Raman, Nile Red, Fourier transform infrared spectroscopy, FT-IR

Introduction

Microplastic (<5 mm) has become a ubiquitous environmental contaminant worldwide[1] since the start of large-scale industrial plastic production during and in the immediate wake of World War II.[2] Annual plastic production reached 233.75 million metric tons (MT) in 2013 and is expected to grow to 334.83 million MT per annum by 2020.[3] Of the 1.3 billion MT of waste generated in urban centers globally in 2010, approximately 21% (275 million MT) was plastic.[4] Most of this plastic waste was managed in energy recovery or landfills, but an estimated 31.9 million MT were classified as mismanaged and therefore a potential source of plastic pollution to the wider environment. An estimated 4.8 to 12.7 million MT of plastic waste entered the ocean in 2010.[4] Early reports of plastic litter in the ocean emerged in the 1970s,[5] with researchers encountering plastic items spanning a variety of sizes from micrometers to meters. Researchers have investigated the abundance of plastic in marine and freshwater environments and the potential effects on associated biota with increasing interest over the ensuing decades, with nearly half of the 17100 citations for "microplastic" emerging since 2014 according to Google Scholar. The predominant focus on aquatic systems has shown microplastic present from remote areas such as polar regions[6] and the deep sea[7–9] to heavily populated urban river catchments,[10,11] estuaries,[12,13] and beaches.[14] Recently, researchers have begun searching farther afield and documenting microplastic in varied systems including floodplain soils,[16] sewage sludge-amended soils,[16,17] subalpine lake sediments in Lake Garda, Italy,[18] and rainwater falling on Paris, France.[19] Discovery of microplastic across so many ecosystems suggests this now-ubiquitous pollutant is yet another marker of the Anthropocene.[20]

Methodological discrepancies exist throughout the marine and freshwater microplastic literature when it comes to identifying microplastic. Research groups have identified microplastic using various combinations of the following methodologies: tactile response, hot wire melt tests, visual quantification, fluorescence after Nile red staining, and spectroscopic methods of μRaman and/ or μFT-IR. These discrepancies largely stem from accessibility, cost, and rapid pace of change within the research community. Given this lack of standardized

DOI: 10.1177/0003702820920652

characterization methods, we set out to evaluate several approaches in a way that could provide guidance to future microplastic researchers.

Recent studies examining microplastic abundance in France's urban Paris[21] and rural Pyrenees mountains[22] concluded that microplastic can be transported through the air and deposited into terrestrial and aquatic environments.[18] Atmospheric deposition is understood as the flux of substances from the atmosphere onto the earth's surface wherein dry and wet deposition combine to produce total atmospheric fallout.[23] Microplastic fallout may prove to be a heretofore underappreciated, major upstream source of microplastic into both terrestrial and aquatic environments. As such, a thorough understanding of the density and distribution of microplastic in air is critical to estimating their potential environmental and human health risks.[23] Airborne microplastic is a potential threat to humans and terrestrial vertebrates when inhaled, respired, and potentially retained within lungs.[19,23–25] Microplastics smaller than 25 μm can enter the human body through the nose or mouth, and those less than 5 μm can end up in lung tissue.[26] Regulatory concern around fine particulates in the air has grown significantly in recent years (e.g., California Air Resources Board's Particulate Matter Program),[27] particularly around the smallest sized anthropogenic fragments linked to a wide range of health impacts including asthma[28] and heart attacks.[29] Most countries have air pollution standards to limit the volumes of fragments less than 10 and 2.5 μm, collectively known as PM 10 and PM 2.5 standards.[26] Interior airspaces within built environments are significant (e.g., the City of Los Angeles alone contains more than 1.7 billion cubic meters of officially recognized structures[27]) and air within such structures could prove to be a microplastic source or sink for the wider environment. The volume of microplastic entering our environment is likely to increase given likely increases in plastic production worldwide.[30]

Three recent studies in France and Germany investigated the density and distribution of microplastic in urban and rural outdoor air.[19,22,23] These studies demonstrated larger fragments present in atmospheric deposition and suggested that local wind-blown debris played a major role in adding to the number of fragments found in bulk samples. Harrison et al.[31] found airborne fragments outside tend to have an upper size limit of 100 μm, whereas fragments in indoor dust are smaller with maximum dimensions around 10 μm.

In this study, we specifically asked (i) whether microplastic loads differ between indoor and outdoor air masses, and (ii) if four different spectroscopic methods produced consistent

DOI: 10.1177/0003702820920652

conclusions. If different methodologies yield different conclusions, some of the recently published work exploring microplastic pollution could be in question.

This research provides evidence of the occurrence of airborne microplastic at California State University Channel Islands (CSUCI), a semi-urbanized landscape in coastal California. We quantified and compared microplastic density (plastic fibers and fragments m^{-3}) between indoor and outdoor air masses, explored different polymer composition within indoor and outdoor air with μRaman and micro-attenuated total reflection Fourier transform infrared microscopy (μATR FT-IR), and suggest some best practices for use of these technologies for the burgeoning field of microplastic characterization.

Methods

Microplastic Nomenclature

Most microplastic we have encountered in various settings in the past three years can be readily classified into one of three gross morphological categories: microspheres (or microbeads, machined spheres with constant diameter designed as abrasives in retail products or industrial processes), fibers (filamentous), and fragments (irregular shaped pieces of plastic often ovoid or trapezoidal). Some research groups distinguish additional fourth category of nurdles (pre-production plastic pellets used as the feedstock for commercial manufacturing); however, in practice we cannot consistently distinguish weathered nurdles from fragments. While we have isolated each of our three common microplastic morphologies from air, this particular data set presented herein captured only fibers and fragments, so our comments will be restricted to these two categories of microplastic.

Air Monitoring Efforts

As part of a larger monitoring effort, we sampled a wide array of air masses across 100 km of coastal Southern California from January 2019 through the end of March 2019. The bulk of this data is being used to characterize human inhalation exposure over the greater coastal zone. For purposes of this paper, we report on a subset of samples collected across the campus of CSU Channel Islands (CSUCI) to compare four microplastic characterization methods; gross visual quantification, fluorescence after Nile red staining, μFT-IR spectroscopy, and μRaman spectroscopy.

DOI: 10.1177/0003702820920652

Sample Locations

Air masses across the CSUCI campus are likely representative of the wider California coastal airshed spanning Santa Barbara and Ventura Counties. CSUCI lies within a wider, semi-urbanized landscape matrix harboring many major industrial, agriculture, and commercial activities nested between densely populated cities and large swaths of natural landscapes/protected areas in coastal southern California. The 337 ha main campus is 8 km inland and sits on the extreme western edge of the Santa Monica Mountains where they intersect with the Oxnard Plain in Ventura County, home to intense row crop, orchard, and greenhouse agriculture. Other major activities within 10 km of campus include large biotechnology, semiconductor, and aerospace clusters, a major military base, a large general aviation airport, and the 101 Freeway corridor (~200000 vehicle trips per day).[29] CSUCI was formally opened in 2002 within the former Camarillo State Mental Hospital campus whose buildings date from the 1930s. As such, occupied University structures are now a diverse matrix of buildings spanning construction dates from 1932 to 2017 with a corresponding mixture of heating, ventilation, and air conditioning systems and environmental envelopes creating a range from interior air masses treated with state of the art air handling and purification systems to spaces with minimal air handling/segregation between external and interior air.

We report data from air sampled air at five locations throughout the CSUCI campus (Table I) between January 2019 and March 2019. At four of these locations, paired air samples were collected to assess microplastics density inside and outside of respective buildings. Two to three replicates were collected at each sampling site, constrained by the logistics of rotating a single sampling apparatus and field researchers' availability. Each air sample was collected during active work week periods (between Monday and Friday) when students were in class session (i.e., excluding breaks or weekends). Each of these sampling sites were within 3–6 m of a building entrance. Outdoor air only was sampled at our fifth site (Student Union Quad), approximately 10 m from the nearest building entrance.

We collected a total of 21 ambient air samples (10 indoor, 11 outdoor) plus their paired procedural controls (n=21) for various levels of analyses: gross traditional microscopy, Nile red stain with fluorescence microscopy, and/or microspectroscopy (μFT-IR or μRaman). While all

DOI: 10.1177/0003702820920652

samples were inspected with gross microscopy and Nile red fluorescence, the distinct sample preparation for μFT-IR and μRaman translated into any given replicate being characterized by either FT-IR or Raman (not both).

Quality Assurance and Quality Control

All measures for microplastic contamination were employed consistently throughout our laboratory and field efforts. First, all researchers handling samples or equipment wore natural fiber clothing at all times in the field and laboratory, with cotton lab coats donned for all sample processing and analysis. Glassware including Petri dishes, vacuum filtration funnels, and tweezers for handling filters, were triple rinsed with doubly filtered deionized (DFDI) water immediately before use. All of our DFDI water utilized for rinsing and sample processing in this study was twice filtered through 1.6 μm filters to remove ambient fragments and plastics present in traditional research-grade deionized water generation systems, thereby reducing sample secondary contamination. Our double filtration yielded water with ≤3.4 microplastic fibers or fragments per liter (3.4±0.4, n=40 L; mean±1 SD). Filters were kept covered at all times after initial sampling, except during imaging and spectrographic characterization steps. Finally, procedural controls were run alongside each sample to quantify contamination from equipment and reagents in samples.

Sample Collection

We sampled airborne microplastic with a simple vacuum filtration array (Fig. 1) that drew ambient air through a glass microfiber filter (GF/A or GF filter; Whatman #1820-047; nominal pore size of 1.6 μm; 47 mm diameter) secured in a vacuum filter holder with a Cole-Parmer Air Admiral vacuum pump (model # P-79202-00). Air flow averaged 11.7 L min^{-1} for a minimum of eight hours, continuously collecting microplastic and other particulates on the GF filter. Extensive preliminary testing showed an eight-hour sample duration guaranteed a sufficient particulate load for analysis. The amount of air pumped through the system was tracked with an airflow totalizer (Alicat Scientific mode # M-100SLPM-D15M) so fragment count could be expressed per volume of air sampled. An average of 4615 L were filtered over the eight-hour sampling windows. Each site was sampled two to three times, with a procedural control included during each sampling event. This procedural control consisted of a second vacuum filter holder

DOI: 10.1177/0003702820920652

with GF filter and vacuum flask, but lacked a pump and added a lid over the filter holder. This covering eliminated any ambient microplastic fallout from the atmosphere. This procedural control served to quantify secondary contamination from equipment, reagents in samples, etc. and allowed us to define our limit of detection (LOD)/quantification (LOQ) for microplastic. Our pumps were plugged into standard electrical outlets to provide a constant voltage, avoiding the sometimes-inconsistent voltage and therefore pump rates that can result from powering such a system with external battery power.

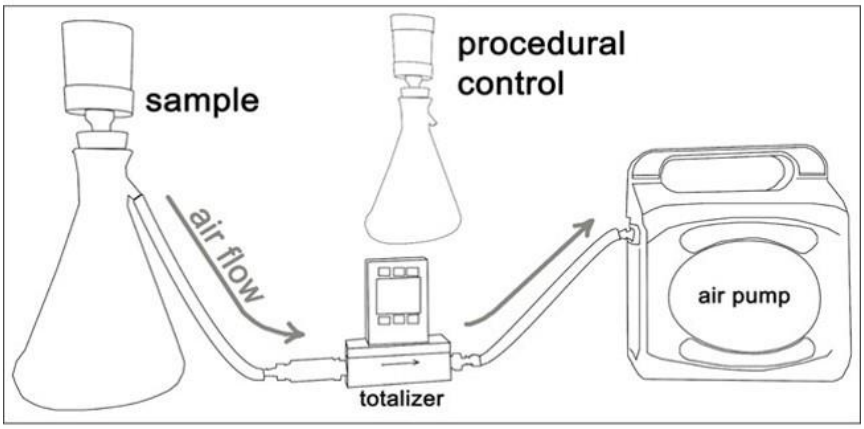

Figure 1. Vacuum filtration setup with filter, filter holder, GF filter (top left), vacuum flask (bottom left), airflow totalizer (middle), and vacuum pump (right). The procedural control was identical to the fist elements, but not connected to a pump and with a cap added over the filter folder. This procedural control was placed adjacent to the sampling array.

Sample Processing

Any microplastics that settled around the inside of the filter holder were rinsed down onto the GF filter with DFDI water at the end of each given round of sampling. We then removed the GF filter from its filter holder, placed it into a cleaned glass petri dish, and immediately covered it. The fibers and fragments collected on GF filters were not put through a digestion procedure to remove organic matter (e.g., cellulose) as we routinely do when analyzing microplastic from other matrices and environments. The fiber and fragment densities on our filters were low enough that we could easily individually visualize and categorize any suspected fragment as plastic, mineral, or other organic matter.

DOI: 10.1177/0003702820920652

Quantification with Traditional Microscopy

In our laboratory, we photographed each GF filter with a stereoscope (Olympus, model SZ61) integrated with a digital camera (Lumenera Infinity 2) under 40x magnification. We then visually quantified particulates embedded on the filter surface after Hidalgo-Ruz,[5] categorizing each by morphology (fiber or fragment) and color. Enumeration followed a consistent, systematic search grid pattern to provide a complete census of the entire filter surface. We scored fragments and fibers as apparent microplastic if they were bright in color, reflective, sharp, fraying or had a length five times their width (standard fiber). Our visual limit of detection (i.e., the smallest fiber or fragment consistently identifiable) was 20 µm.

Quantification with Microscopy and Nile Red

Nile red can improve quantification of microplastics because it is a lipid soluble fluorescent dye that stains hydrophobic materials.[32,33] Following our visual quantification, we exposed our filters to 0.5–1 mL of 10 µg/mL of Nile red solution (made up as 1 mg/mL in acetone and diluted in n-hexane).[34] Filters were allowed to dry with the upper petri dish lid slightly askew in the fume hood for a minimum of 10 min. We again quantified apparent microplastic on these stained filters under a 450–510 nm LP fluorescent light (Orion-Lite 455 nm #OL-455NG) for excitation and an orange 529 nm filter for viewing subsequent fluorescence.[32] Fibers and fragments were scored as microplastic if they fluoresced under these conditions.

Microplastic Morphometrics

All fibers and fragments upon 20 randomly selected filters (six indoor air samples, ten outdoor air samples, two indoor procedural controls, and two outdoor procedural controls) were measured with an NIH Image Fiji.[35] We measured the total length of each fiber and maximum width for each fragment. While NIH Image can batch process large numbers of targets via automated routines, the diversity of target morphologies drove us to conduct all measurements manually. Length and width data were log transformed to better meet assumptions of normality and then compared with one-way analysis of variance (ANOVA) with SPSS (IBM v.24.0.0.0) software.

Spectrographic Characterization

DOI: 10.1177/0003702820920652

We further characterized a subset of the fibers and fragments found on the GF filters by micro-Raman (μRaman) and micro-Fourier transform infrared (μFT-IR) spectroscopy. Both of these spectrographic methods have been applied to characterize fibers and fragments isolated from different matrices and confirm the presence of microplastic.[22,36,37] Furthermore, these two methods are complementary,[38–40] with each yielding somewhat different information about the fibers and fragments isolated from air in this study.

μRaman Spectroscopy

We generated spectra of Raman shifts in the 200–2000 range with a Horiba Scientific Xplora Plus confocal Raman microscope (Raman shift: 50–3200 cm, 1.5 cm^{-1} resolution, imaging accuracy 0.5 μm) with a motorized *x*,*y*,*z* stage. Our general settings consisted of a 785 nm laser at 25–100% power (filter), 1200 mm^{-1} gratings with a 100 μm split, and 10–15 s acquisition times (i.e., fiber and fragment exposure to the laser) and five to 10 accumulations (averaged to generate a final spectrum). We adjusted our default settings to maximize signal strength and minimize fluorescence and damage to the fibers and fragments being examined. Two other laser wavelengths, 532 nm and 683 nm, were available and spectra were attempted with them. However, with the sample presentation used here and in the majority of analyses conducted, our strongest signal and minimum fluorescence were observed with the 785 nm laser. Higher laser power (i.e., 50% and 100%) and the higher energy lasers (i.e., 532 nm and 683 nm) were more likely to burn the fiber and fragment being examined.[22,41] Spectrum from any fiber or fragment burned during analysis were not utilized and the item was re-analyzed in a different area if possible. There were, however, a number of fibers that withstood the 785 nm laser at 100% with no visible damage.

We selected, at random, 155 fibers and fragments from five indoor and six outdoor filters for individual Raman analysis, generating 23 usable spectra for indoor samples and 44 usable spectra for outdoor samples. We had less usable spectra from Raman analysis compared to FT-IR because of high fluorescence and burning of fibers and fragments. Four procedural control filters were similarly examined under our Raman confocal microscope, with a Raman spectrum generated for each fiber or fragment encountered. In addition, two GF filters stained only with Nile red (no other processing), were examined in the same manner (termed Nile red blanks).

DOI: 10.1177/0003702820920652

Raman spectra were analyzed through the Bio-Rad ExpertID software (18.3.111.0) with KnowItAll spectral databases AnalyzeIt Raman (18.3.111.0). The baseline and noise correction factors available via ExpertID were applied to process raw spectra prior to library searches. Composite spectra (two to four component) with a library-sample-match of $\geq 90\%$ were utilized.

μ*FT-IR Spectroscopy*

Our μFT-IR analysis used a Thermo Scientific Nicolet iN10Mx microscope. Because glass fibers yield a strong signal IR signal, fibers and fragments could not be analyzed on the original GF filters used for collection. Instead, fibers and fragments were removed from the GF filters and spread out on a glass slide with a stream of DFDI water. The fibers and fragments were allowed to completely dry and then individually analyzed with a germanium micro-attenuated total reflection (ATR) interface on the FT-IR microscope with a mercury–cadmium–telluride (MCT) detector. The smooth background of the slide did not interfere with micro-ATR analyses, whereas the 3D textured glass fibers pose issue with reflection measurements. Spectra were collected at a resolution of 8 cm^{-1} and 64 scans were coded to yield a final absorbance spectrum from 650–4000 cm^{-1}.

The FT-IR spectra baselines were corrected, and the spectra analyzed through ThermoFisher OMNIC Picta software (v.1.7) populated with extensive polymer spectral databases. Spectra yielding a single component library-sample-match of >90% are reported here. We selected four indoor and four outdoor air filters spanning our sampling locations for FT-IR analysis. From these filters we characterized 121 fibers and fragments via FT-IR, generating 59 usable spectra from indoor and 62 from outdoor samples.

Reported Microplastic Density

Unless stipulated as “raw” microplastic counts, all reported microplastic density data herein are adjusted to reflect potential contamination. For blank correction, we subtracted the relevant (i.e., indoor fiber, indoor fragment, outdoor fiber, or outdoor fragment) contaminant load present on a paired procedural control from the raw microplastic counts measured upon our experimental filters, yielding the corrected microplastic loads. Further, all fiber and fragment counts on each filter were divided by the volume of air pumped through the filter, as recorded by the airflow

DOI: 10.1177/0003702820920652

totalizer in standard liters, multiplied by a 10^3 conversion factor and reported as fibers or fragments per m^3.

Results

Background Contamination

Our procedural controls had median values of 8.1 fibers and 4.7 fragments present on the indoor sample filters (n=10) and 0.6 fibers and 7.3 fragments per outdoor sample (n=11) when assessed with gross microscopy. These procedural controls had an aggregate (fibers + fragments) microplastic contamination of 12.8 ± 4.0 (mean ± 1 SD) across all indoor filters and 12.0 ± 3.4 across all outdoor filters, translating into a contamination load of less than one microplastic item per 2.9 cm^2 of filter area. Our Nile red procedural controls had median values of 2.4 fibers and 12.2 fragments per indoor filter (n=10) and 0.4 fibers and 6.3 fragments per outdoor filter (n=11). Aggregate (fibers + fragments) Nile red controls harbored 5.3±5.1 microplastic items per filter.

We used the above fiber and fragment values to correct our raw microplastic densities out of an abundance of caution. However, we were only able to confirm a single polymer (a red fragment from an outdoor control) upon our procedural control filters with Raman and FT-IR spectroscopy. All other items (n=13) successfully characterized from our control filters were mineral, carbon, or some other non-plastic material. In short, our contamination control procedures for polymer contamination were effective and our corrections provide a conservative overall estimate of microplastic abundance.

Fiber and Fragment Sizes

Fiber lengths did not differ significantly ($F_{1,301}$=2.017, p=0.157) between indoor (641±810.7 µm, mean ± 1SD) and outdoor (616±536.7 µm) air masses, although our largest fibers were found indoors (Table II). Maximum indoor fiber length (8961 µm) was more than four times longer than the largest outdoor fiber (2061 µm) encountered. Our most abundant fiber length category was 101–301 µm for both indoor (26.6±0.1% of all indoor fibers) and outdoor (29.7±0.1% of all outdoor fibers) air masses (Fig. 2).

In contrast, fragments were significantly ($F_{1,280}$=46.866, p<0.001) smaller in inside buildings. Outdoor (104.8±64.9 µm) microplastic fragments were nearly twice as large as their

DOI: 10.1177/0003702820920652

indoor (58.6±55 µm) counterparts on average (Table II). As with all of the fiber distributions we observed, outdoor fragments were most abundant at intermediary size ranges with 39.2±0.1% of fragments in the 76–100 µm range (Fig. 2). Indoor fragments were strongly dominated by the smallest size classes with 59.2±0.1% in our smallest size range (<50 µm) and followed a strongly exponential distribution.

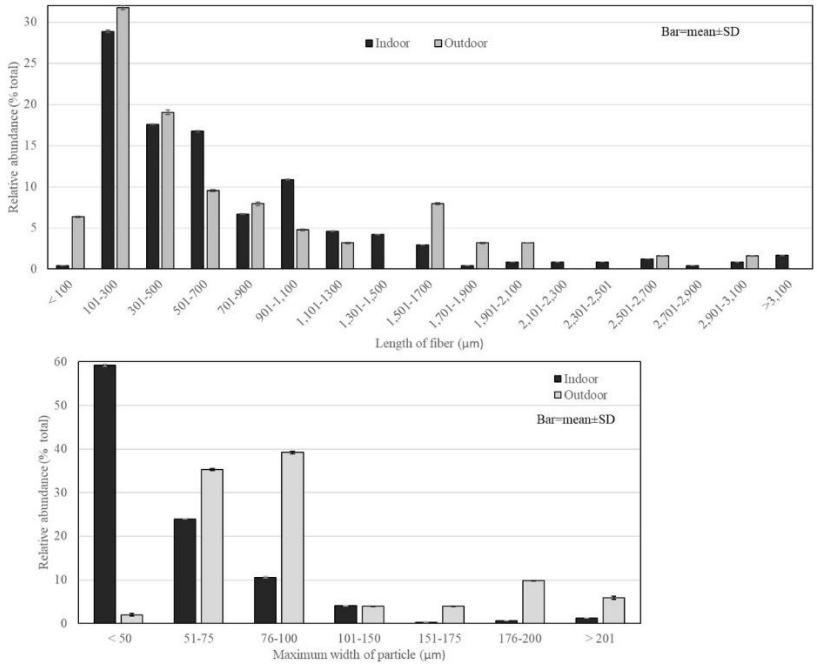

Figure 2. Size distribution for all fibers (top) and fragments (bottom) counted and measured on sample GF filters. Bins are 25 µm for fragments and 200 µm for fibers (due to the greater range of sizes). Bars: mean ± 1SD.

Traditional Microscopy: Fibers

Interior air spaces were significantly enriched with microfiber relative to outdoor spaces ($F_{1,20}$=13.757, p=0.001; Fig. 3, Table III). Gross visual microscopy counts showed indoor air contained many more fibers (9.8±7.3 fibers per m³; mean±1 SD) than outdoor (1.5±1.1 fibers per m³). Indoor sites segregated into relatively fiber-dense and fiber-sparse locations. The Broome Library foyer (17.0±3.8 fibers per m³) and Sierra Hall main entrance (15.4±3.1 fibers per m³) were fiber-rich spaces and our Modoc (3.0 ±0.6 fibers per m³) and ESRM (3.2 ±0.4 fibers per m³) laboratories were comparatively fiber-poor.

DOI: 10.1177/0003702820920652

Outdoor microfiber abundance was comparable to our low-fiber interior spaces, but all outside fiber concentrations were below the levels of all sampled interior spaces. Outdoor fibers fluctuated little between our facilities parking lot (adjacent to our Modoc laboratory; 2.2±01.8 fibers per m^3), campus mall (1.7±0.7 fibers per m^3), ESRM patio (1.3±0.2 fibers per m^3), Student Union plaza (1.1±0.7 fibers per m^3), and Broome fountain (0.7±0.1, fibers per m^3).

Traditional Microscopy: Fragments

Interior air spaces had significantly fewer microplastic fragments relative to outdoor spaces ($F_{1,20}$=12.500, p=0.002; Fig. 3, Table III). In aggregate, interior spaces had roughly half (6.7±5.2 fragments per m^3) the fragments of outdoor (15.5±6.1 fragments per m^3) regions. In descending rank, interior fragment densities were; Broome Library foyer (8.3±6.3 fragments per m^3), ESRM laboratory (7.9±5.6 fragments per m^3), Sierra Hall foyer (6.7±6.8 fragments per m^3), and Modoc laboratory (2.7±2.7 fragments per m^3).

Outdoor microplastic fragment abundance ranged from highs of 19.6±2.0 (Broome fountain) and 18.1±7.9 (Facilities parking lot) to 13.2±5.6 (ESRM patio), 12.9±2.4 (campus Mall), and 12.5±10.6 (Student Union plaza) fragments per m^3.

Traditional Microscopy: Apparent Diversity

The apparent diversity of aggregated fibers and fragments was greater in interior spaces (Fig. 3), primarily due to more evenly distributed categories. Black fragments strongly dominated outdoor air microplastics, accounting for 45% of the total outdoor items observed.

DOI: 10.1177/0003702820920652

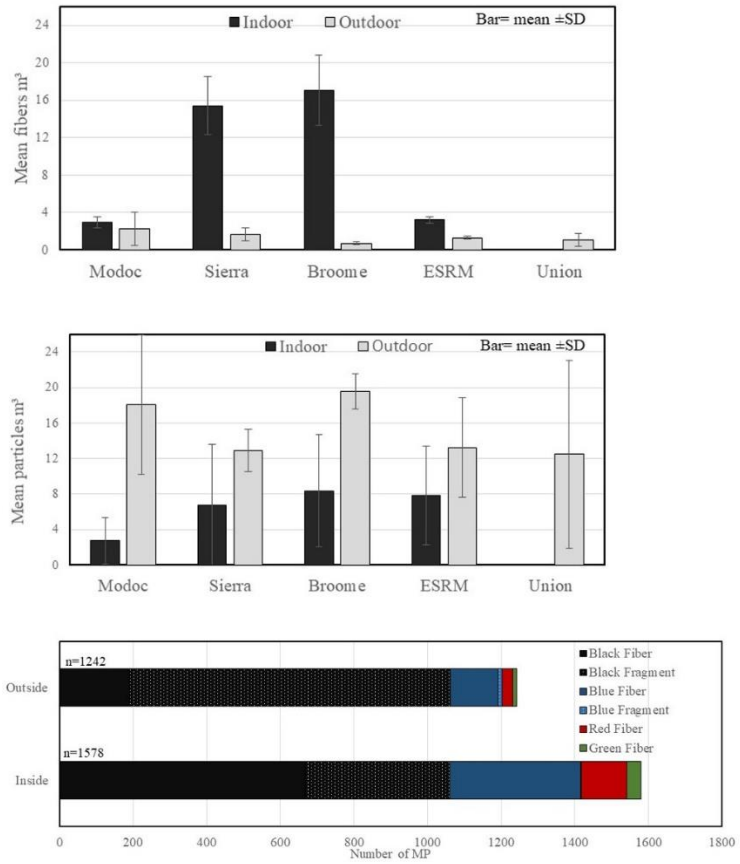

Figure 3. Microplastic fiber (top) and fragment (middle) counts per m^3 of air sampled across CSUCI from traditional microscopy. Bars: mean ± 1 SD. Abundance of the total number of microplastics (bottom) fibers (solid) and fragments (dotted) counted across all sample GF filters binned by color (left to right: black, blue, red, green).

Nile Red Fluorescence

Samples processed with Nile red mirrored the trends already described between indoor and outdoor microfiber, but with only approximately one-third of the microplastic counts observed with gross microscopy (Table III). Indoor air again harbored significantly ($F_{1,20}$=31.358, p<0.001) more microfiber (3.3±2.9 fibers per m³; mean±1 SD) than outdoor (0.6±0.6 fibers per m³; Fig. 5). For microplastic fragments however, the indoor-outdoor pattern inverted itself such that interior spaces (12.6±8.0 fragments per m³) now showed twice the fragment abundance as outdoor (5.6±3.2 fragments per m³) spaces, a significant difference ($F_{1,20}$=13.055, p=0.004). As

DOI: 10.1177/0003702820920652

with our microfibers, absolute fragment counts were also approximately one-third of the estimates from gross microscopy for our outdoor samples. The increase in fragments counted upon our indoor filters with Nile red was driven by many exceedingly small items (generally <10 µm). These exceedingly small fragments stained/fluoresced strongly and were therefore much easier to detect and count compared to our bright field approach used with the previous gross microscopy technique. In short, our enumeration ability greatly improved with these bright objects on a dark background (e.g., Fig. 4).

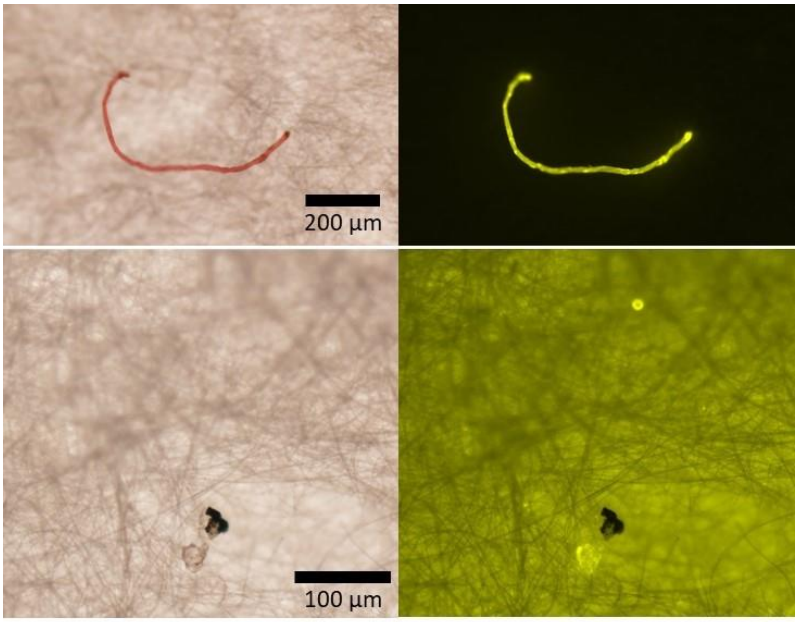

Figure 4. Examples of Nile red stained microplastics under ambient light (left) and blue light (455 nm) viewed with an orange filter (529 nm; right)

DOI: 10.1177/0003702820920652

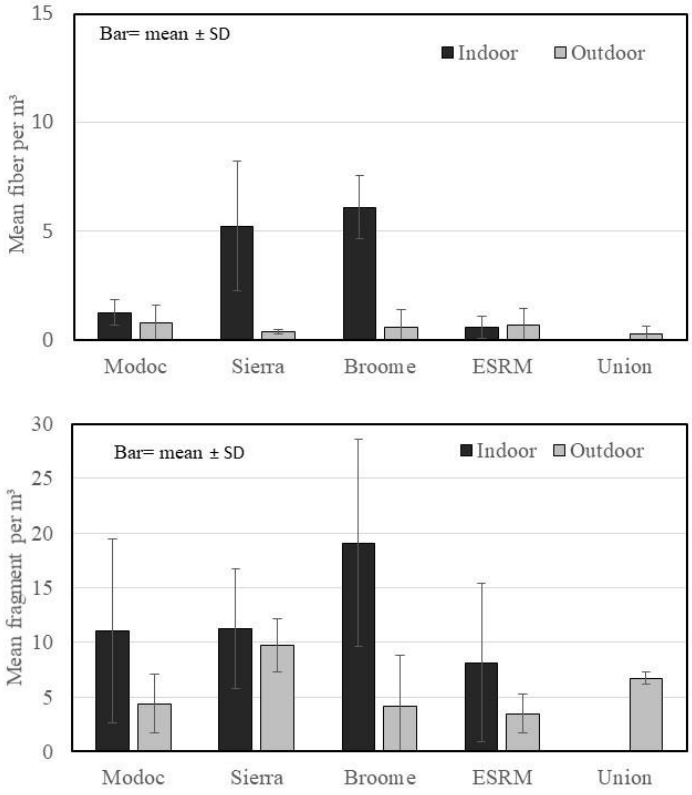

Figure 5. Microplastic fiber (top) and fragment (bottom) density per m³ of air sampled across CSUCI from microscopy with Nile red. Bars: mean ± 1 SD.

Chemical Composition Spectroscopy: µFT-IR

Our 122 fibers and fragments successfully characterized with µFT-IR spectroscopy (Fig. 6) were dominated by non-plastic compounds (90%, n=110), including inorganic substances (46%, n=56) and cellulose (45%, n=54; Fig. 7b, Table III). Polystyrene (PS) dominated (46%, n=5) aggregate µFT-IR plastic polymer signals with polyethylene terephthalate (PET; 36.4%, n=4), polyethylene (PE; 9%, n=1), and acrylic (9%, n=1) also encountered. Micro-FT-IR painted a rather homogeneous landscape of plastics both indoors and out. Indoor plastic polymers consisted of PS (n=4) and PET (n=3). We encountered only singleton spectra from polymers (PET, PS, and acrylic) on outdoor filters (Fig. 7d, Table III).

Chemical Composition Spectroscopy: µRaman

Of the 71 fibers and fragments we successfully characterized with µRaman spectroscopy (Fig. 6), 38 (54%) were synthetic plastic polymers. The remainder were fingerprinted as non-polymer

DOI: 10.1177/0003702820920652

anthropogenic substances (15%, n=11), mineral or cellulose (24%, n=17), and dyes or simply unknown (7%, n=5; Fig. 7a, Table III). Polyvinyl chloride heat stabilizer (PVC-HS) was the most common plastic detected overall with μRaman, comprising 50% (n=19) of our identified plastics and dominating both indoor (n=7) and outdoor (n=12) plastic signals. Polymetric plastic additives (polymeric) comprised 24% (n=9) of our aggregate plastic items. All other plastics were detected only once or twice: polyvinyl chloride (PVC; 5%, n=2), polyethylene (PE; 5%, n=2), resin (5%, n=2), acrylic (6%, n=2), polycarbonate (PC; 3%, n=1), and polystyrene (PS; 3%, n=1; Fig. 7d, Table III).

Our various air masses presented generally similar plastic compounds as characterized by μRaman. Indoor plastic polymers primarily consisted of PVC-HS 47% (n=7), polymeric 40% (n=6), and PE 13% (n=2). Outdoor plastic polymers were similar, consisting of 57% (n=12) PVC-HS, 10% (n=2) PS, and 10% (n=2) polymeric.

Plastic Identifiers

Our spectrographic characterizations did not always rely on a "pure" polymer signal itself. We frequently utilized spectra of additives associated with a given commercial formulation of a plastic item's identity. Our most common plastic identifiers were PVC additives (52%, n=19), Dibutyl-dichlorotin (79% n=15) and Valfor 100 Zeolite (21%, n=4), both common heat stabilizers in PVC.[37] Another common spectrum (n=4) was the polymeric additive polyphosphoric acid (PPA) used to improve the properties of polymer-modified asphalts.[42] The polymeric additive 1,2,3 triazole (n=4) is a photostabilizer in polymers with strong antimicrobial and antifouling properties integrated into many plastics but most commonly into polystyrene.[43] We also encountered the copper phthalocyanine (n=1) dye used in various polymers.[37] The remaining plastic spectra were common "pure" plastic polymer signals of PVC (n=2), PE (n=2), Resin (n=2), Acrylic (n=1), PC (n=1), and PS (n=1).

DOI: 10.1177/0003702820920652

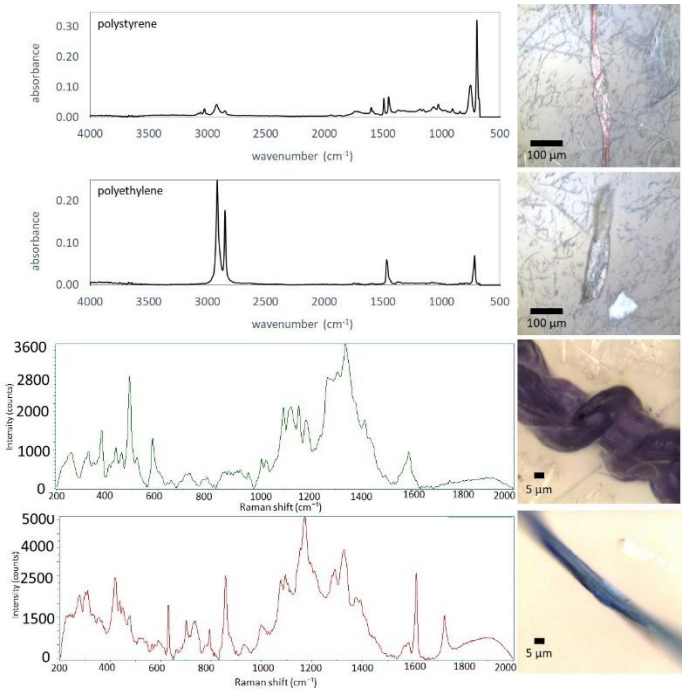

Figure 6. Representative images and spectra from µFT-IR (top two panels) and µRaman (bottom two panels).

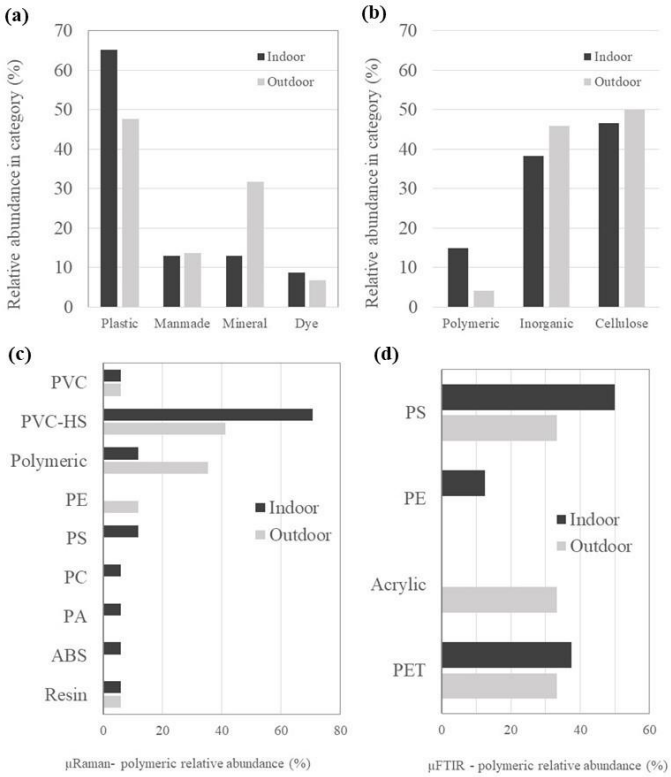

DOI: 10.1177/0003702820920652

Figure 7. Abundance of different materials detected using µRaman (a) and µFT-IR (b), and relative abundance of the different polymeric materials detected using µRaman (c) and µFT-IR (d) in subsampled fragments and fibers. PVC=polyvinyl chloride, PVC-HS=polyvinyl chloride-heat stabilizer, PE=polyethylene, PS=polystyrene, PC=polycarbonate, PA=polyamide, ABS=acrylonitrile butadiene styrene, PET=polyethylene terephthalate.

Discussion

Amounts of Microplastics in Air

Visual Quantification. Our results confirm the ubiquitous presence of microplastic in indoor and outdoor air environments demonstrated in previous studies.[13,19,21–23,44–46] Note these previous studies have sampled both microplastics suspended in air (via vacuum filtration) and microplastic fallout from air (via bulk deposition samples). This present study focused on the former (suspended microplastic) as a potential direct exposure pathway to humans. Suspended indoor air microplastic densities on the CSUCI campus from traditional microscopy, 9.8±7.3 fibers per m^3 and 6.8±5.2 fragments per m^3, are comparable to the two previous studies: 5.4 fibers per m^3 (median) and 9.3±5.8 fragments+fibers per m^3.[13,21] CSUCI outdoor air suspended microplastic densities, 1.5±1.1 fibers per m^3 and 15.5±6.1 fragments per m^3 are consistent with one previous study, 0.9 fibers per m^3 (median).[21] The only other study published to date on suspended outdoor microplastic densities reported inconsistently high values of 1274±390 total microplastic (fragments+fibers) per m^3.[46] This final estimate is three orders higher than anything we have sampled in this or any of our other airborne microplastic monitoring across the United States (unpublished data), lacked controls, and lacked verification that the substances that were collected were indeed polymers.

We measured significantly elevated concentration of fibers inside ($F_{1,20}$=13.757, p=0.001), with 6.5 times greater density (quite similar to the 5.5x estimate from Nile red estimates), on average, inside compared to outside air. Dris and coworkers[21] reported a similar trend with fiber densities in indoor (6x greater than outdoor) air. Indoors, clothes made of synthetic materials, furniture, carpets and air filters are all potential sources of fibers to air and exist at a higher concentration than outside. Further, inside air has less of a chance of mixing with fresher/cleaner air and reduced dilution propensity compared to turbid outdoor air masses. Traditional microscopy showed suspended fragment densities were 2.3x greater outdoors than

DOI: 10.1177/0003702820920652

indoors. The majority of our fragments found both indoor and outdoor were black, but many were not identifiable with either Raman or FT-IR spectroscopy (either retuning no useful spectra or manifesting as “black carbon”). Intriguingly, at least some of these small black fragments could ultimately prove to be trace amounts of tire according to a recent study published by the San Francisco Estuary Institute wherein they state, “nearly half of the fragments from field [water and sediment] samples were black fragments. Spectroscopic analysis and secondary characteristics suggested these fragments might be synthetic or natural rubber”.[47]

Nile Red Quantification

Our microplastic density estimates from Nile red counts varied in comparison to densities from traditional microscopy. The same filters used during visual quantification were stained with Nile red and subsequently counted under a blue light with an orange filter. Both indoor and outdoor fiber and outdoor fragment densities decreased by a factor of 2.5–3.0 with Nile red counts (Table III). This decrease demonstrates the selectivity of the hydrophobic Nile red that stains synthetic fibers and fragments and selected organic matter, but not inorganic or hydrophilic materials. Previous studies with Nile red staining of microplastics have reported that cotton cellulose, wool, paper products, “black carbon”, algae, and other OH-rich carbohydrate-based polymers only stain weakly.[32,48] Other biogenic materials, such as chitin, wood lignin, and natural waxes can stain strongly and may lead to false positive counts when such compounds are abundant.[32,49] Considering that 42–47% of the fibers examined under µFT-IR were cellulose (Table III) and would likely not stain (or stain weakly), a decrease in fiber counts is consistent with our understanding of and experience with Nile red methodology and efficacy. Outdoor fragments likely comprise a variety of plant matter fragments, some of which will stain, so more data is needed to investigate the observed trend in terms of selectivity. Further, the decrease in Nile red counts may also demonstrate the selectivity of Nile red to different polymer types. For example, PP, PE, and PS stain strongly, but PC, PET, PVC and weathered PE stain to a lesser extent.[49] PVC and PET were strong components of the polymeric makeup in µRaman and µFT-IR analyses (Fig. 7), respectively, and may have only weakly stained; they thereby may well have been undercounted in our Nile red enumeration.

We saw a markedly distinct pattern with indoor fragments and Nile red, which was the exact opposite of the trends for fibers and outdoor fragments. Nile red counts for indoor

DOI: 10.1177/0003702820920652

fragments almost doubled compared to traditional microscopy. One possibility for the increase is the staining of chitin material; however, this outcome would be a better explanation in outdoor air where fragments of arthropod exoskeletons and similar biogenic materials are presumably more abundant. A second, more likely possibility is that Nile red improves the accuracy of smaller, clear, and white fragment counts. Beyond the ability to selectively stain plastics, we have found Nile red improves counts of smaller-sized fragments by creating a clearer fluorescing signal on a dark background that is more easily visible and counted, something observed by other researchers as well.[32,34,49] Maes et al.[32] predict that fragments down to 5 µm may potentially be visualized, depending upon the optics of the microscope in use. Further, Nile red will illuminate clear and white fragments that are obscured by the GF (or any other light colored) filter background. In our study, indoor air appears to have a concentration of small fragments that were stained and more accurately counted under fluorescing conditions. The possibility that these fragments are of biogenic origin, rather than polymeric, cannot be ruled out, as no digestion step was carried out. Nevertheless, the large quantity of small fragments quantified with Nile red is consistent with the indoor air fragment size distributions (Fig. 2) where small fragments <50 µm comprise 59.2±0.1% of our overall sample pool.

Spatial Variation of Microplastics in Air

Microplastic fiber densities varied between the five sampled sites on the CSUCI campus, while the fragment densities stayed generally consistent between sites (Fig. 3). The most notable trend is higher fiber densities encountered at our Sierra Hall foyer and Broome Library sites, and lower densities at our Modoc, ESRM and Union sites. The Sierra and Broome sites connect well-used areas of the campus, are major throughways for students and staff, and thus sustains high foot traffic. Fibers from the synthetic clothing of students and staff passing through could easily contribute to microfiber loading of the inside air. With estimates of 1900 to 250 x 10^3 fibers per garment being released during a single wash cycle[50,51] of synthetic clothing, fibers being broken and shedding as a person crosses a throughway is quite reasonable and a likely source of fibers at the Sierra and Broome sites. In-progress work by our research group is currently accumulating evidence that supports this interpretation of fiber shed in high-traffic or densely populated interior spaces.

DOI: 10.1177/0003702820920652

Size of Microplastics in Air

Fragments were more abundant than fibers in both indoor and outdoor air. Of the 668 individual microplastic targets measured on sample filters, 366 were fragments and 302 were fibers. This is consistent with previous studies that reported microplastic fragments as the major components in atmospheric fallout.[22,23] Also similar to previous work, fiber and fragment distributions show highest abundance within smaller size classes and reduced abundance of larger size categories more easily seen with lower magnifications and more readily manipulated with traditional tools. Indoor air fragments sizes appear to be following a trend different from outdoor fragments and all fibers, indoor and out.

The accuracy of fiber and fragment counts decreases approaching our (size) limit of detection (20 μm). Our data indicate a larger pool of smaller fragments (moving toward nanoplastics), consistent with other work,[21–23] that we likely poorly (if at all) quantified here. These are an important size class, as these smallest fragments (<5 μm) are the most inhalable and respirable in terrestrial mammal lungs.[52]

We observed a number of notable differences in microplastic size distributions between outdoor and indoor air. First, the size range of fibers and fragments in outdoor air (fiber 25-2061, fragment 51–408 μm) were smaller than for items in indoor air (fiber 22–8961 μm, fragments 20–850 μm), although overall fiber lengths did not differ significantly (p=0.157) between indoor and outdoor areas. It is possible that indoor fibers and fragments undergo less weathering (less exposure to UV sunlight, wind, temperature shifts, etc.) and are thereby somewhat less likely to fracture than those in outdoor air, potentially explaining the maximum interior fiber size being more than four times the length of correspondingly outdoor fibers. Further, the stable, low-wind indoor conditions inside buildings will allow these larger fibers and fragments to more easily settle out than in the turbid outdoor environment. Dris et al.[21] reported a similar trend with fibers (50–1650 μm for outdoor air and 50–3250 μm for indoor air) but their maximum fiber lengths were more than half the size of this study. Dris et al.[21] sampled air masses at 1.2 m, an average breathing height, while our study pumped air only 30 cm off the ground. Larger fibers with greater mass and surface area may lack sufficient buoyancy to reach the 1.2 m breathing height, and might settle more rapidly or more readily gather on surfaces,[22] including this study's GF filter resting at just 30 cm off the ground. As always, the different sampling locations (private

DOI: 10.1177/0003702820920652

European apartments versus North American university campus) may also influence these observed differences in fiber length.

Second, and most notably, <50 µm fragments dominate our indoor air (59%), while 50–100 µm fragments are more abundant in outdoor air (62%). As recognized with our Nile red analyses, small fragments appear to be concentrating within indoor air. Indoor air has concentrated sources of fragments (skin cells, tracked-in dirt, fragments from paper goods and plastic packaging, etc.) that are not as easily diluted as outdoor air. Further, the central HVAC systems in most of the university buildings sampled employed Merv10 filter (or better) rated to remove >85% of 3–10 µm fragments and 50–65% of 1–3 µm fragments. As air is cycled through the HVAC system, some smaller fragments may not be removed, settle as dust and resuspend, or be cycled back through the HVAC, thereby concentrating in indoor air.

Composition of Microplastics in Air

Our chemical characterization of sampled fibers and fragments with parallel µRaman and µFT-IR show differences in the polymeric makeup between indoor and outdoor air (Fig. 7). The fibers and fragments evaluated during µFT-IR analysis were 15% polymeric outdoor and 5% indoor; the parallel µRaman analysis values were 63% polymeric indoor and 47% outdoor (Fig. 7). The consistent trend between these methods was the greater polymeric abundance in indoor air particulates. The remaining content was natural (e.g., cellulose and wool), inorganic (e.g., minerals), or simply unidentified materials (Fig. 7).

The relative contributions of polymeric and cellulosic material indoors shown with FT-IR data (Fig. 7) is lower than the two previous indoor air studies that reported 33% and 50% polymeric material[21] and 67% and 50% natural fiber.[14] The dominant polymer also differs between studies. In this study, FT-IR data was dominated by PS, followed by PE and PET. Vianello et al.[13] reported PE as the dominant polymer in their samples, while Dris et al.[19] found PP most abundant. Further, the Raman data from this study shows PVC as most prevalent, followed by PE.

Outdoor air also had an abundance of natural materials with lower contributions from polymeric materials (43% cellulose, 5% polymeric; FT-IR, Fig.7). FT-IR data showed an equal distribution of PS, acrylic and PET polymers, yet Raman data was dominated again by PVC signals (Fig. 7). Kaya et al.[46] reported that PE and polyamides were most abundant in their

DOI: 10.1177/0003702820920652

outdoor air samples. No other studies, to our knowledge, have chemically characterized suspended microplastics in outdoor air. Studies that have examined microplastic fallout in outdoor air reported PE, ethylene vinyl acetate (EVAS), PET, PE, PP and PS as the major polymers identified using FT-IR,[23,44] and PS, PE, and PP using Raman.[22]

Many factors influenced these results from sample location to sample processing and terminal analysis. Terminal analysis, which can be defined the end analysis for further understanding of combined analyses. For example, Vianello et al.[13] and Dris et al.[20] sampled in private apartments and rooftops in large urban European cities, whereas our study evaluated a semi-urban university campus surrounded by multiple land uses (urban cities, agriculture, protected areas, etc.). It is reasonable to expect the sources of plastic, and thus the atmospheric loading, to vary between these quite different sampling locations. Next, each FT-IR analysis was carried out with different modes (reflectance versus transmission) and on different substrates (glass slide versus zinc selenide window), which can bias signal strength from different size, shape and type of polymer. Studies used different terminal analyses: FT-IR and Raman. FT-IR and Raman signals are often complementary, and it has been documented that PE shows a strong signal in FT-IR and, oppositely, PVC yields a strong signal in Raman.[38,39]

Overall, our data show that the distribution of polymer type varies between indoor and outdoor air. The FT-IR and Raman data together indicate that PE and PET polymer abundance is greater inside, while PVC and acrylic are found more outside. PE and PET are common in food packaging (plastic bags and water bottles, to-go containers) and construction materials (vapor barriers, window films, flooring protection), but most notably as textiles (synthetic clothing, fleece sweaters and blankets).[51] PVC fibers are widely used in outdoor furniture and coverings due to their ease of use and durability. Non-fibrous PVC has many other applications, but the PVC microplastics identified here were mainly fibrous.

Insights from Multiple Microscopy Methods

Each of the four microscopy methods applied to microplastic fibers and fragments sampled from air on the CSUCI campus provide different insights into microplastic sources, pathways and composition. Traditional microscopy allows gross counts of microplastic densities and assessment of microplastic morphology (shape, size distribution, etc.), but misidentification can lead to large errors.[53] Nile red staining with microscopy provides selectivity of plastics and a

DOI: 10.1177/0003702820920652

lower (size) limit of detection that improves upon traditional microscopy, although it is not a perfect “plastic only” stain. Raman and FT-IR work together to chemically fingerprint sampled fibers and fragments. Chemical fingerprints allow for source tracking and investigations of microplastic pathways into the environment. While FT-IR can identify many polymer types and natural and inorganic materials (cellulose, wool, silicates), generating a sufficient signal from small diameter fibers or fragments (<20 μm) is limited and detecting trace components (<1%) requires complex sample preparation. Raman, in addition to identifying many polymer types, can be extremely sensitive to trace components, such as dyes and additives, that can further help fingerprint and allow upstream or downstream source tracking of sampled fiber and fragment populations. However, in some cases, the dye and additive fingerprints can overwhelm the polymeric signal. For example, Raman analysis of an acrylic paint chip in Kappler et al.[39] revealed a titanium oxide colorant not visible with IR, but required parallel FT-IR analysis to pinpoint the underlying acrylic polymer. In this study, FT-IR provided a strong fingerprint of major components comprising subsampled fibers and fragments (cellulose, inorganic, PS, PE, PET, acrylic), while Raman gave a more detailed fingerprint of the dyes and additives associated with polymeric and synthetic materials (Fig. 7 and Table III). Dyes and additives in synthetic material can pose a health risk[54] and the level of detail provided by Raman analysis as to their presence may be important for risk assessments of human exposure to microplastic.

Recommendations for Future Studies

As expected, a post hoc review of the four microscopy methods employed in this study reveal a number of potential improvements for future studies. Because the field of microplastic quantification and characterization is in rapid development and no standardized methods have been globally adopted, it is important to practically share such lessons learned with the greater scientific community. In this way, the field can move together to prudently compile robust standardized methods. With such a sentiment in mind, we share our lessons learned during this study and share resulting recommendations in detail below.

Sample Presentation

When compiling a study design for microplastic evaluations in any environment, it is important to choose the terminal analysis ahead of time. The four microscopy methods applied in this

DOI: 10.1177/0003702820920652

study, traditional microscopy, Nile red staining and microscopy, and characterization via μFT-IR or μRaman, as well as chemical characterization via pyrolysis–gas chromatography–mass spectrometry (GC-MS), are increasingly common terminal analyses.[55,56] The ideal sample presentation varies between these terminal analyses and the study design should consider methods that minimize sample processing and yield the optimal sample presentation for their chosen terminal analysis.

The initial terminal analysis chosen for this study was traditional microscopy, for which the use of GF filters was appropriate. The GF filters were low-cost, clean, easy to use (strong, not brittle and do not tear easily) and provided a clean white background for easy visualization of collected microplastic. One disadvantage is that white and clear plastics are less visible on the white background provided. On the other hand, any filter type will obscure some category of plastic. The GF filters were compatible with Nile red and thus we were easily able to move forward with Nile red staining and subsequent fluorescent microscopy.

The GF filters showed varying compatibility with μFT-IR and μRaman (discussed below). However, for both μFT-IR and μRaman, it is useful to present the microplastic for characterization on a filter paper/membrane that has a smooth surface, in terms of texture and 3D character. Accumulating microplastic on smooth and flat filters improves the quality and efficiency of μFT-IR and μRaman analyses, as well as the ability of confocal microscopes to focus during visual examination and photo-documentation of samples. GF filters are comprised of overlapping glass microfibers and present a rough and textured surface. Fragments can embed in the microtopography of such 3D textured surfaces, impeding their characterization, and the textured background of the filter itself can prevent the use of fragment-finder software that depends on strong microplastic-filter contrast for reliable use. Oppositely, polycarbonate filters, have a smooth uniform surface with little 3D character. Any filter's texture can be easily checked under a microscope at the magnification chosen for terminal analysis[57] and we encourage novice researchers to do so. Lastly, different sample processing steps can warp filters, sometimes permanently, no longer permitting them to lie flat. Of greatest concern here is the "ridging" which can occur when using vacuum filter funnels that have an elevated and textured platform. We suggest researchers use traditional borosilicate glass vacuum filter platforms that are uniform and flat.

DOI: 10.1177/0003702820920652

Working Solutions

We are just on the cusp of our wider scientific microplastic community more broadly acknowledging that working solutions used in the sample processing steps can be a significant source of secondary contamination[32,36,58,59] in microplastic samples and, thus, all working solutions must be pre-filtered using filter pore-sizes less than that detected by the specific study's terminal analysis. Surprisingly, this includes Milli-Q treated deionized (DI) water; water from the Millipore system used in this study has on average 3.4 microplastics per L (Fig. 8a) and requires double filtering prior to use with samples.

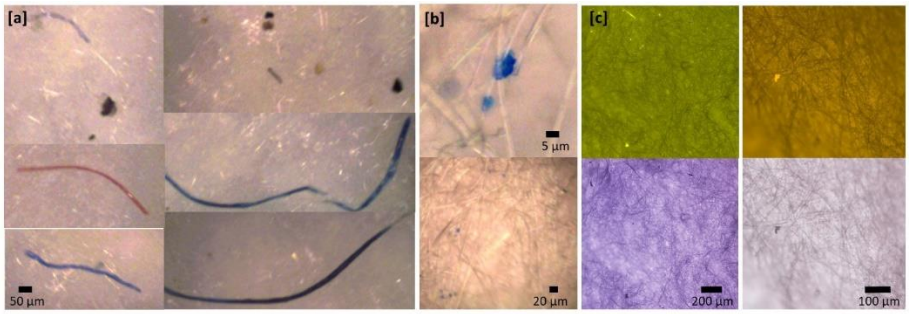

Figure 8. Representative photographs of different contaminants. Select fibers and fragments filtered out of "raw" (i.e., not doubly filtered) (a) Milli-Q deionized water, (b) one cluster of secondary contamination encountered on a Nile red stained filter, and (c) fluorescent (top) and visual (bottom) pictures of a GF filters dyed with Nile red.

The Nile red used in this study was not pre-filtered, which was an oversight. It was made up with high-performance liquid chromatography (HPLC)-grade acetone and n-hexane in DFDI pre-rinsed glassware. This level of good laboratory practice did not suffice. One of the two Nile red blank fibers visually examined under the Raman confocal microscope was clean, while the other yielded a single patch of small blue fragments (Fig. 8a). Nile red is likely a source of heterogenic secondary contamination that can easily be eliminated via pre-filtering in future studies.[32]

Terminal Analyses

FT-IR Microscope. FT-IR microscopes are a powerful tool that can capture the polymeric signal of microplastics, cellulose and other materials.[38,39,60,61] These microscopes have several

DOI: 10.1177/0003702820920652

configurations to interface with samples: transmission mode (requiring samples placed within IR transparent windows), ATR using various sized refractive crystals in direct contact with samples, and reflection mode. In addition, several detector configurations are available with differences in sensitivity, expense and speed: deuterated triglycine sulfate (DTGS), MCT, MCT-linear arrays, and focal point array (FPA; multiple detector elements in a large array). For application to microplastic research, transmission and µATR with a signal MCT detector (faster and higher sensitivity compared to DTGS) are useful for larger fragments and fibers that can be readily picked from environmental samples and placed in transmission cells or on a sturdy surface in contact with a µATR crystal. Smaller fragments and fibers (<100 µm) that challenging to move can be analyzed via µATR on their original collection surface.

Whole filters with areas from 95 to 1735 mm^2 (i.e., circular filters with diameters of 11 to 47 mm) that are used to isolate fragments and fibers from environmental matrices require a different approach. With environmental matrices, it is common that hundreds of fragments and fibers are isolated on a filter and/or items <100 µm in size are abundant on the filter. Under such conditions, it is not practical or physically possible to move each item on the filter into a transmission cell for analysis. Further, it is time prohibitive to move item by item with a µATR crystal cleaning in between each measurement. Indeed, there are various sized µATR crystals available with contact areas in the 0.008 to 0.8 mm^2 range (corresponding to 0.1 to 1 mm crystal diameters) that can be coupled with FPA detectors and utilized in fast mapping modes. However, to map a 95 mm^2 filter with a 0.8 mm^2 ATR would require >100 contact points on the filter, with cleaning needed between each measurement and the risk that any given contacted item could be removed and lost from the sample during crystal clearing. And, the heterogeneity of fragments and fibers on a filter in terms of thickness and malleability make it difficult to establish a consistent pressure of each item against a larger ATR crystal.

For filters, operating in reflection mode with an MCT linear array or FPA detector, which can collect multiple spectra over a larger area at once, is more practical. For example, the Thermo Fisher Nicolet iN10 MCT linear array comprises a 2 x 8 array of MCT elements and, through automation, can map a 1.2 x 1.2 mm area in 4.5 minutes with a 25 x 25 µm spatial resolution, 16 cm^{-1} spectral resolution, and 1 scan per location. In this mode, fully mapping an 11 mm filter will require roughly six hours and produce a considerably large spectral data set. Looking forward, condensing or altering sample volumes samples to end with a smaller diameter

DOI: 10.1177/0003702820920652

filter and techniques for filter subsampling will be important to improve efficiency.[22,62] Another promising approach is reducing the area of a filter that is analyzed via fragment finder software, which minimizes the amount of data generated per filter and improves spectral quality as specific fragments are targeted rather than mapping the gross area of a filter. Challenges with reflection mode include textured fragments or fibers with high refractive indices can interfere with IR signals,[39] and more significant, the signal from the filter material can interfere with the spectra of the fragment or fiber given that many common filters have a strong IR signal (e.g., cellulose acetate, glass microfiber). Gold coated filters provide the optimal substrate with minimal IR signal and reflective properties that improve the fragment or fiber IR signal. Pricewise gold filters may be cost prohibitive for many labs and other options, such as silica, aluminum oxide and reusable gold coated slides are being investigated.[13,62–65]

Additional considerations with μFT-IR involve signal character, general interferences, and detection limits. FT-IR is a bulk technique such that it is easier to characterize components at percentage levels meaning, in plastics, the polymer itself will often give a stronger signal than the trace components such as dyes and additives. The weaker signal from dyes and additive can require further sophisticated sample preparation in compression cells followed by analysis in transmission mode and possibly spectral subtraction or multicomponent spectral matches to reference spectra in databases for detection. Certain materials, such as glass fibers, silicate minerals, and water yield strong signals that can interfere with important polymeric fingerprint regions. Further, FT-IR is considered resolution-restricted to larger fragments and fibers >10–15 μm due to limits in diffraction of the source light and physical contact between the ATR crystal and sample.[60,65] While ATR can push this diffraction limit with high refractive index crystals like Germanium and collect a spectrum from objects as small as 1 μm (paired with a sensitive detector), these are practical for point measurements on selected fragments or fibers. In this study, interference from glass microfibers drove our use of a μATR coupled with a single MCT detector on selected fragments and fibers removed from our GF filters to obtain clear and identifiable spectra.

Raman Microscope

Raman complements FT-IR well in that it is an excellent tool for examining small fibers and fragments (<20 μm) as well as characterizing dyes and additives that comprise a small portion of

DOI: 10.1177/0003702820920652

a material's chemical makeup.[38,39,60] Challenges associated with Raman include developing an ideal sample presentation, minimizing fluorescence, and working in conjunction with signals from dyes and additives that overlay the polymeric backbone (these signal issues are quickly being addressed with new method development, technological advancements, and mathematical corrections).[41] Our experience with each of these aspects in this study are outlined below. Common substrates used for sample presentation with μRaman at present include polycarbonate, aluminum coated polycarbonate, aluminum oxide, silicon filters or glass slides, gold coated glass slides, and glass petri dishes.[40,57] Note that gold coated polycarbonate filters are only useful if they are stretched flat. Any warping of the surface leads to strong contrast and interferes with location of fragments on the filter surface when viewing through the confocal microscope. These substrates work to minimize background noise and fluorescence, while maximizing Raman signal and microplastic-filter contrast.[57] In this study, the original GF filters from the sample collection process were used for sample presentation on the μRaman. The use of the original filters prevented any microplastic loss or secondary contamination that may occur during transfer to a new filter material. Further, those glass microfibers on GF filters readily break and transfer with the microplastic to the new filter material. The presence of transferred glass microfibers can interfere with microplastic characterization. That said, our GF filters were reasonably compatible with μRaman. The Raman signal from two different fibers (one from DI water and one from an air sample) was tested under different conditions: (i) on a dry GF filter, (ii) on a wet GF filter, and (iii) on a glass slide. We accomplished this by carefully moving the fibers with a pair of fine tweezers from surface to surface. The glass slide yielded the strongest signal, followed by the wet GF filter and then the dry GF filter (Fig. S1, Supplemental Material). Additionally, wetting the GF filter allowed the glass microfibers to flatten, reducing their 3D nature, improving the focus of the confocal microscope and reducing the glass microfiber interference with the Raman signal from microplastics.

As mentioned in other studies, the interference of fluorescence with the Raman signal is a general challenge in microplastic characterization.[38,41,57] Raman signals can be 10^4 to 10^8 less efficient than fluorescent signals,[66] especially in strongly colored plastic or plastic containing fluorescent dyes. This challenge can be met with several approaches that are described in Araujo et al.[41] These approaches involve the application of different laser wavelengths, photobleaching, variation in sample presentation (e.g., aluminum polycarbonate filters)[57] and algorithms to

DOI: 10.1177/0003702820920652

remove fluorescent signals from spectra.[40] Unfortunately, fluorescent signals that overpowered the Raman signal leading to highly elevated baselines were frequent in our sample set and attempts at different laser wavelengths and/or intensities were only sometimes useful. This decreased the overall number of successful spectra we were able to generate.

Plastics that are colored, but not fluorescent at the laser wavelength used for analysis, can yield strong Raman spectra; however, the Raman signal from dye or additives in the plastics may overpower the Raman signal of the polymeric material (e.g., Käppler et al.[39]). In this study, multicomponent library searches of the KnowItAll database with Bio-Rad ExpertID software were dominated by dyes and additives, with low to no signal from the polymeric backbones. Subtracting the dye spectra from the original sample spectra yielded clearer polymer matches only in some cases, indicating the interference from the dye signal was too strong to pull out the polymer signal in many cases. Dyes and additives are associated with most manufactured materials and (when associated with specific materials) provide relevant information for characterization of fibers or fragments from challenging environmental matrices.[39] For example, dibutyl dichlorotin is a heat stabilizer associated with PVC that was frequently detected in our samples (Table S1).

We evaluated a spectral range of 200–2000 cm^{-1}, similar to several previous studies.[22,37] However, for future studies, moving to a range of 400–3200 cm^{-1} may be more effective at capturing the microplastic polymeric backbone.[23,36,39,40] There is a cluster of Raman peaks in the 2780–2980 cm^{-1} range resulting from CH–CH–CH_2 groups stretching vibrations and are strongly exhibited by many of our more common plastics (Figure 4 in Käppler et al.[39]). The obvious downside here is that such a wider spectral window can double to triple analysis time as the full 400–3200 cm^{-1} range cannot be captured in a single detector window. Two to three windows would need to be analyzed and coadded (depending on the excitation laser used). This additional analysis time would need to be evaluated and weighed against the quality of spectra produced and their ability to identify polymeric signals.

Nile Red Staining

Aluminum oxide membrane and polycarbonate filters are commonly used with Nile red for sample presentation,[32–34] however, the original GF sample filters used in this study were easily adapted to Nile red. The glass microfibers are compatible with the n-hexane and acetone solvents

DOI: 10.1177/0003702820920652

within the Nile red staining solution and other than some secondary contamination from the Nile red solution (Fig. 8), do not appear to have any significant fluorescent interference under the conditions utilized in the study (Fig 8). A check of the planned sample presentation is important because fluorescent interference can occur and add to background noise.[34] During traditional microscopy of GF sample filters, yellow organic-like material (often irregularly elongated along one axis and "lumpy") and degraded carbonaceous material (black carbon) were observed. This black carbon had no fluorescent signal, while the yellow organic-like matter had an infrequent, but variable fluorescent signal suggesting possible algal or other microbial origins. These observations, along with the high abundance of cellulose shown in the FT-IR data, indicate a digestion step to reduce the presence of organic material prior to Nile red staining is necessary for suspended air samples. As with all of our other microplastic work, a digestion step for airborne sampling will likely improve the overall accuracy of visual and Nile red counts, given that our original secondary contamination can be minimized. Overall, Nile red quantification that includes a sample digestion step and is initially validated with FT-IR or Raman characterization and matrix spikes,[32] can provide an approachable method for evaluating microplastic contamination densities in environmental samples.

Conclusion

This study presents some of the first data on microplastic densities in air, specifically comparing indoor and outdoor environments. Suspended fibers and fragments were filtered from air for subsequent microplastic analysis in paired, indoor and outdoor locations around the CSUCI campus in coastal California. Sampled fibers and fragments were assessed for microplastic content using four microscopy techniques that are presently being evaluated by the larger scientific community for their effectiveness in the field of environmental microplastic contamination. Each technique was able to provide different information about the source, pathway, and/or composition of our sampled microplastic. Traditional microscopy, the most broadly used technique, was useful for gross counts of microplastic density, investigations into the different microplastic morphologies present, and especially with observations of spatial trends across the university campus. We found elevated fiber densities in indoor areas with high foot traffic, potentially from microfibers shedding off synthetic clothing. Fluorescent microscopy with a pre-digestion and Nile red staining, as well as prior method validation, can improve the

DOI: 10.1177/0003702820920652

accuracy of traditional microscopy. In our case, Nile red counts picked up a large population of small (<50 µm) indoor air fragments that would otherwise not have been visualized or counted. Because no digestion was carried out in the study, we cannot rule out the biogenic origin of these small fragments as opposed to a polymeric origin, but their presence is an interesting observation that stemmed from Nile red staining.

The two spectrographic techniques we employed, µFT-IR and µRaman, showed PE and PET fibers concentrated indoors where people and furniture with synthetic PE and PET clothing are also concentrated and air is minimally diluted with fresher/cleaner air masses. Outside, we observed an abundance of PVC fibers common to exterior fabric and canvas. These chemical fingerprinting techniques are, as present, only semi-automated and require a certain skill set to produce high quality spectra and subsequent fingerprints. Thus, a number of recommendations on sample preparation/presentation, instrument setup and technique strengths and weaknesses are included herein as a resource to novice users.

Airborne microplastic represents a potential direct pathway for human plastic exposure and an underappreciated source of microplastic transport into distant terrestrial and aquatic ecosystems. As such this and similar studies highlight the need for comparable, robust global data on the varying densities of microplastics in air as well as improved estimates of human exposure, acute and chronic toxicities related to respired microplastics, and potential mechanisms and policies for future source reductions. The multiple assessment techniques applied herein will each be important in providing a more coherent picture of microplastic contamination in air as our nascent field of environmental microplastic characterization works towards these larger goals.

Acknowledgments

The authors would like to thank Ralph Diego, recent graduate of California State University Channel Islands (CSUCI) for his non-stop collection of indoor and outdoor air samples; Eunah Lee, Horiba Raman Project Manager at HORIBA Scientific, for training, mentoring, and use of the µRaman instrument; Andrew Whitley, VP Sales and Business Development at HORIBA Scientific for providing us with this opportunity; CSUCI Students: Julie McHorney, Emmie Wordin, Nathan Shaprio, and Melvin Kim for helping in various tasks as needed to complete the data analysis, and lastly the Cause and Tracy S. Hanna Scholarship for supporting Ralph Diego’s

data collection.

References

1. D.K. Barnes, F. Galgani, R. C. Thompson, M. Barlaz. “Accumulation and Fragmentation of Plastic Debris in Global Environments”. Philos. Trans. R. Soc., B. 2009. 364(1526): 1985–1998.
2. V.E. Yarsley, E.G. Couzens. Plastics. Hammondsworth; Middlesex: Penguin, 1945.
3. Grand View Research. "Plastics Market Analysis by Product (PE, PP, PVC, PET, Polystyrene, Engineering Thermoplastics), by Application (Film and Sheet, Injection Moulding, Textiles, Packaging, Transportation, Construction) and Segment Forecast to 2020". 2014. https://www.radiantinsights.com/research/plastics-market-analysis-by-product-pe-pp-pvc-pet-polystyrene-engineering-thermoplastics-by-application-film-amp-sheet-injection-molding-textiles-packaging-transportation-construction-and-segment-forecasts-to-2020 [accessed 30 Mar 2020].
4. J. Jambeck, R. Geyer, C. Wilcox, T. Siegler, et al. “Plastic Waste Inputs from Land into the Ocean”. Science. 2015. 347(6223): 768–777.
5. V. Hidalgo-Ruz, L. Gutow, R.C. Thompson, M. Thiel. “Microplastics in the Marine Environment: A Review of the Methods Used for Identification and Quantification”. Env. Sci. Technol. 2012. 46(6): 3060–3075.
6. M. Bergmann, V. Wirzberger, T. Krumpen, C. Lorenz, et al. “High Quantities of Microplastic in Arctic Deep-Sea Sediments from the HAUSGARTEN Observatory”. Environ. Sci. Technol. 2017. 51(19): 11000–11010.
7. M. Claessens, L. Van Cauwenberghe, M.B. Vandegehuchte, C.R. Janssen. “New Techniques for the Detection of Microplastics in Sediments and Field Collected Organisms". Mar. Pollut. Bull. 2013. 70(1–2): 227–233.
8. A.J. Jamieson, L.S.R. Brooks, W.D.K. Reid, S.B. Piertney, et al. “Microplastics and Synthetic Particles Ingested by Deep-Sea Amphipods in Six of the Deepest Marine Ecosystems on Earth”. R. Soc. Open Sci. 2019. 6(2): 180667.
9. L.C. Woodall, C. Gwinnett, M. Packer, R.C. Thompson, et al. “Using a Forensic Science Approach to Minimize Environmental Contamination and to Identify Microfibers in Marine Sediments”. Mar. Pollut. Bull. 2015. 95(1): 40–46.

DOI: 10.1177/0003702820920652

10. R.R. Hurley, A.L. Lusher, M. Olsen, L. Nizzetto. “Validation of a Method for Extracting Microplastics from Complex, Organic-Rich, Environmental Matrices". Environ. Sci. Technol. 2018. 52(13): 7409–7417.
11. P. Kay, R. Hiscoe, I. Moberley, L. Bajic, N. McKenna. “Wastewater Treatment Plants as a Source of Microplastics in River Catchments”. Environ. Sci. Pollut. Res. Int. 2018. 25(20): 20264–20267.
12. X. Peng, M. Chen, S. Chen, S. Dasgupta, et al. “Microplastics Contaminate the Deepest Part of the World’s Ocean”. Geochem. Perspect. Lett. 2018. 9: 1–5.
13. A. Vianello, R.L. Jensen, L. Liu, J. Vollertsen. “Simulating Human Exposure to Indoor Airborne Microplastics Using a Breathing Thermal Manikin”. Sci Rep. 2019. 9(1): 8670.
14. D. Horn, M. Miller, S. Anderson, C. Steele. “Microplastics are Ubiquitous on California Beaches and Enter the Coastal Food Web Through Consumption by Pacific Mole Crabs”. Mar. Pollut. Bull. 2019. 139: 231–237.
15. M. Scheurer, M. Bigalke. “Microplastics in Swiss Floodplain Soils”. Environ. Sci. Technol. 2018. 52(6): 3591–3598.
16. F. Corradini, P. Meza, R. Eguiluz, F. Casado, et al. “Evidence of Microplastic Accumulation in Agricultural Soils from Sewage Sludge Disposal”. Sci. Total Environ. 2019. 671: 411–420.
17. K.A. Zubris, B.K. Richards. “Synthetic Fibers as an Indicator of Land Application of Sludge”. Environ. Pollut. 2005. 138(2): 201–211.
18. H.K. Imhof, N.P. Ivleva, J. Schmid, R. Niessner, C. Laforsch. “Contamination of Beach Sediments of a Subalpine Lake with Microplastic Particles”. Curr. Biol. 2013. 23(19): R867–868.
19. R. Dris, J. Gasperi, M. Saad, C. Mirande, B. Tassin. “Synthetic Fibers in Atmospheric Fallout: A Source of Microplastics in the Environment?” Mar. Pollut. Bull. 2016. 104(1–2): 290–293.
20. Subcommission on Quaternary Stratigraphy. Working Group on the 'Anthropocene'. 2019. http://quaternary.stratigraphy.org/working-groups/anthropocene/ [accessed 30 Mar 2020].
21. R. Dris, J. Gasperi, C. Mirande, C. Mandin, et al. “A First Overview of Textile Fibers, Including Microplastics, in Indoor and Outdoor Environments”. Environ. Pollut. 2017. 221: 453–458.

DOI: 10.1177/0003702820920652

22. S. Allen, D. Allen, V.R. Phoenix, G. Le Roux, et al. “Atmospheric Transport and Deposition of Microplastics in a Remote Mountain Catchment”. Nat. Geosci. 2019. 12(5): 339–344.
23. M. Klein, E.K. Fischer. “Microplastic Abundance in Atmospheric Deposition Within the Metropolitan Area of Hamburg, Germany”. Sci. Total Environ. 2019. 685: 96–103.
24. S. Atis, B. Tutluoglu, E. Levent, C. Ozturk, et al. “The Respiratory Effects of Occupational Polypropylene Flock Exposure”. Eur. Respir. J. 2005. 25(1): 110–117.
25. A. Churg, M. Brauer. “Ambient Atmospheric Particles in the Airways of Human Lungs”. Ultrastruct. Pathol. 24(6): 353–361.
26. S. Wright, F. Kelly. “Plastic and Human Health: A Micro Issue?”. Environ. Sci. Technol. 2017. 51(12): 6634.
27. California Air Resources Board. "Particulate Matter Program". 2015. https://ww3.arb.ca.gov/desig/pm.htm [accessed 30 Mar 2020].
28. C.A. Keet, J.P. Keller, R.D. Peng. "Long-Term Coarse Particulate Matter Exposure is Associated with Asthma among Children in Medicaid”. Am. J. Respir. Crit. Care Med. 2017. 197(6): 737–746.
29. Y. Du, X. Xu, M. Chu, Y. Guo, J. Wang. “Air Particulate Matter and Cardiovascular Disease: The Epidemiological, Biomedical, and Clinical Evidence”. J. Thoracic Dis. 2016. 8(1): E8–E19.
30. D. McKay. "Fossil Fuel Industry Sees the Future in Hard-to-Recycle Plastic". Conversation. 2019. https://theconversation.com/fossil-fuel-industry-sees-the-future-in-hard-to-recycle-plastic-123631 [accessed 30 March 2020].
31. J.K. Gietl, R. Lawrence, A.J. Thorpe, R.M. Harrison. “Identification of Brake Wear Particles and Derivation of a Quantitative Tracer for Brake Dust at a Major Road”. Atmos. Environ. 2010. 44(2): 141–146.
32. T. Maes, R. Jessop, N. Wellner, K. Haupt, A.G. Mayes. “A Rapid-Screening Approach to Detect and Quantify Microplastics Based on Fluorescent Tagging with Nile Red”. Sci Rep. 2017. 7: 44501.
33. T. Stanton, M. Johnson, P. Nathanail, R.L. Gomes, et al. “Exploring the Efficacy of Nile Red in Microplastic Quantification: A Costaining Approach”. Environ. Sci. Technol. Lett. 2019. 6(10): 606–611.

DOI: 10.1177/0003702820920652

34. K.J. Wiggin, E.B. Holland. “Validation and Application of Cost and Time Effective Methods for the Detection of 3–500 μm Sized Microplastics in the Urban Marine and Estuarine Environments Surrounding Long Beach, California". Mar. Pollut. Bull. 2019. 143: 152–162.

35. J. Schindelin, C.T. Rueden, M.C. Hiner, K.W. Eliceiri. “Golden Opportunitites: A Horizon Scan to Expand Sandy Beach Ecology”. Mol. Reprod. Dev. 2015. 82(7–8): 518–529.

36. A.K. Kniggendorf, C. Wetzel, B. Roth. “Microplastic Detection in Streaming Tap Water with Raman Spectroscopy”. Sensors. 2019. 19(8): 1839.

37. S. Zhao, M. Danley, J.E. Ward, D. Li, T.J. Mincer. “An Approach for Extraction, Characterization and Quantitation of Microplastic in Natural Marine Snow Using Raman Microscopy”. Anal. Methods. 2017. 9(9): 1470–1478.

38. L. Cabernard, L. Roscher, C. Lorenz, G. Gerdts, S. Primpke. “Comparison of Ramana and Fourier Transform Infrared Spectroscopy for the Quantification of Microplastics in the Aquatic Environment”. Environ. Sci. Technol. 2018. 52(22): 13279–13288.

39. A. Kappler, D. Fischer, S. Oberbeckmann, G. Schernewski, et al. “Analysis of Environmental Microplastics by Vibrational Microspectroscopy: FT-IR, Raman or Both?”. Anal. Bioanal. Chem. 2016. 408(29): 8377–8391.

40. J. Wagner, Z.-M. Wang, S. Ghosal, C. Rochman, et al. “Novel Method for the Extraction and Identification of Microplastics in Ocean Trawl and Fish Gut Matrices”. Anal. Methods. 2017. 9(9): 1479–1490.

41. C.F. Araujo, M.M. Nolasco, A.M.P. Ribeiro, P.J.A. Ribeiro-Claro. “Identification of Microplastics Using Raman Spectroscopy: Latest Developments and Future Prospects”. Water Res. 2018. 142: 426–440.

42. F. Zhang, C. Hu, Y. Zhang. “The Effect of PPA on Performances and Structures of High-Viscosity Modified Asphalt”. J. Therm. Anal. Calorim. 2018. 134(3): 1729–1738.

43. R.N. Sasidhar Kantheti, K.V.S.N Raju. “The Impact of 1,2,3-Triazoles in the Design of Functional Coatings”. RSC Adv. 2014. 5: 3687–3708.

44. L. Cai, J. Wang, J. Peng, Z. Tan, et al. “Characteristic of Microplastics in the Atmospheric Fallout from Donguan City, China: Preliminary Research and First Evidence”. Environ. Sci. Pollut. 2017. 24(32): 24928–24935.

DOI: 10.1177/0003702820920652

45. S. Dehghani, F. Moore, R. Akhbarizadeh. “Microplastic Pollution in Deposited Urban Dust, Tehran Metropolis, Iran”. Environ. Sci. Pollut. 2017. 24(25): 20360–20371.

46. A. Tunahan Kaya, M. Yurtsever, S. Çiftçi Bayraktar. “Ubiquitous Exposure to Microfiber Pollution in the Air”. Eur. Phys. J. Plus. 2018. 133(11): 488.

47. R. Sutton, D. Lin, M. Sedlak, C. Box, et al. “Understanding Microplastic Levels, Pathways, and Transport in the San Francisco Bay Region”. Richmond, Calif.: SFEI Contribution No. 950. San Francisco Estuary Institute, 2019. https://www.sfei.org/documents/understanding-microplastics [accessed 30 March 2020].

48. J.C. Prata. “Airborne Microplastics: Consequences to Human Health?”. Environ. Pollut. 2018. 234: 115–126.

49. M. Tamminga. “Nile Red Staining as a Subsidiary Method for Microplastic Quantification: A Comparison of Three Solvents and Factors Influencing Application Reliability”. J. Earth Sci. Environ. Studies. 2017. 2(2): 165–172.

50. M.A. Browne, P. Crump, S.J. Niven, E. Teuten, et al. “Accumulation of Microplastic on Shorelines Worldwide: Sources and Sinks”. Environ. Sci. Technol. 2011. 45(21): 9175–9179.

51. U. Pirc, M. Vidmar, A. Mozer, A. Kržan. “Emissions of Microplastic Fibers from Microfiber Fleece During Domestic Washing”. Environ. Sci. Pollut. Res. 2016. 23(21): 22206–22211.

52. J. Gasperi, S.L. Wright, R. Dris, F. Collard, et al. “Microplastics in Air: Are We Breathing It In?”. Curr. Opin. Environ. Sci. Health. 2018. 1: 1–5.

53. M. Eriksen, S. Mason, S. Wilson, C. Box, et al. “Microplastic Pollution in the Surface Waters of the Laurentian Great Lakes". Mar. Pollut. Bull. 2013. 77(1–2): 177–182.

54. J.H. Weisburger. Mutation Research 376. “A Perspective on the History and Significance of Carcinogenic and Mutagenic N-Substituted Aryl Compounds in Human Health”. Mutat. Res. 1996. 376(1–2): 261–266.

55. W. Cowger, et al. Journal of Spectroscopy, in Review (2019).

56. E. Holland, et al. Journal of Spectroscopy, in Review (2019).

57. B.E. Ossmann, G. Sarau, S.W. Schmitt, H. Holtmannspotter, et al. “Development of an Optimal Filter Substrate for the Identification of Small Microplastic Particles in Food by Micro-Raman Spectroscopy”. Anal. Bioanal. Chem. 2017. 40(16): 4099–4109.

DOI: 10.1177/0003702820920652

58. G. Erni-Cassola, M.I. Gibson, R.C. Thompson, J.A. Christie-Oleza. “Lost, but Found with Nile Red: A Novel Method for Detecting and Quantifying Small Microplastics in Environmental Samples”. Environ. Sci. Technol. 2017. 51(23): 13641–13648.

59. F. Kroon, C. Motti, S. Talbot, P. Sobral, M. Puotinen. “A Workflow for Improving Estimates of Microplastic Contamination in Marine Waters: A Case Study from North-Western Australia”. Environ. Pollut. 2018. 238: 26–38.

60. "Guide to the Identification of Microplastics by FT-IR and Raman Spectroscopy". Thermo Fisher Scientific White Paper WP53077, 2018. https://assets.thermofisher.com/TFS-Assets/MSD/Application-Notes/WP53077-microplastics-identification-ftir-raman-guide.pdf [accessed 30 March 2020].

61. I.R. Comnea-Stancu, K. Wieland, G. Ramer, A. Schwaighofer, B. Lendl. “On the Identification of Rayon–Viscose as a Major Fraction of Microplastics in the Marine Environment: Discrimination Between Natural and Manmade Cellulosic Fibers Using Fourier Transform Infrared Spectroscopy”. Appl Spectrosc. 2017. 71(5): 939–950.

62. M.G.J. Löder, M. Kuczera, S. Mintenig, et al. “Focal Plane Array Detector-Based Micro-Fourier-Transform Infrared Imaging for the Analysis of Microplastics in Environmental Samples”. Environ. Chem. 2015. 12(5): 563–581.

63. S. Primpke, C. Lorenz, R. Rascher-Friesenhausen, G. Gerdts. “An Automated Approach for Microplastics Analysis Using Focal Plane Array (FPA) FT-IR Microscopy and Image Analysis”. Anal. Methods. 2017. 9(9): 1499–1511.

64. S.M. Mintenig, I. Int-Veen, M.G.J. Löder, S. Primpke, G. Gerdts. “Identification of Microplastic in Effluents of Wastewater Treatment Plants Using Focal Plane Array-Based Micro-Fourier-Transform Infrared Imaging”. Water Res. 2017. 108: 365–372.

65. A. Kappler, F. Windrich, M.G.J. Löder, M. Malanin, et al. “Identification of Microplastics by FT-IR and Raman Microscopy: A Novel Silicon Filter Substrate Opens the Important Spectral Range Below 1300 cm(–1) for FT-IR Transmission Measurements”. Anal. Bioanal. Chem. 2015. 407(22): 6791–6801.

66. P.M. Pellegrino, E.L. Holthoff, M.E. Farrell. Laser-Based Optical Detection of Explosives. Boca Raton, Florida: CRC Press, 2015.

DOI: 10.1177/0003702820920652

Tables

Table I. Air sampling locations on the California State University Channel Islands campus (Camarillo, California). Note: for simplicity, the "pair" descriptor will be used in subsequent data figures.

Pair	Indoor sites			Outdoor sites		
	Location	Descriptor	Replicates	Location	Descriptor	Replicates
Modoc	Modoc	Laboratory	2	Facilities	Parking lot	3
Sierra	Sierra	Foyer	2	Mall	Promenade	2
Broome	Broome	Library	3	Fountain	Reflecting pool	2
ESRM	ESRM	Laboratory	3	Patio	Terrace	2
Union	–	–	–	Union	Plaza	2

Table II. Size of airborne microplastic fibers and fragments at CSUCI. Note: these measurements exclude items smaller than 20 μm.

DOI: 10.1177/0003702820920652

	Fiber length (µm)					Fragment size (µm)				
	n	Min	Max	Mean	SD	*n*	Min	Max	Mean	SD
Indoor	239	22	8961	641	810	316	20	850	58	55
Outdoor	63	25	2061	616	536	50	51	408	104	64

Table III. Summary of the mean and standard deviation (SD) of all sample GF filters analyzed in each category and the polymeric content of the fragment and fiber subset analyzed by µFT-IR and µRaman. Note the raw and blank (i.e., procedural control) corrected values for visual and Nile red counts are included. Were we to have conducted a digestion of filters, the cellulose signals would have disappeared, so we present these for ease of comparison with other publications.

	Indoor per m^3		Outdoor per m^3	
	Fiber (mean ± SD)	Fragment (mean ± SD)	Fiber (mean ± SD)	Fragment (mean ± SD)
Visual quantification				
Raw	11.4 ± 7.8	7.6 ± 4.8	2.6 ± 1.4	16.5 ± 6.0
Corrected	9.8 ± 7.3	6.8 ± 5.2	1.5 ± 1.1	15.5 ± 6.1
Nile red quantification				
Raw	3.8 ± 2.9	14.6 ± 8.5	1.0 ± 0.8	6.6 ± 3.3
Corrected	3.3 ± 2.9	12.6 ± 8.0	0.6 ± 0.6	5.6 ± 3.2
Spectrographic characterization				

DOI: 10.1177/0003702820920652

	Indoor Air Fiber + Fragment Polymeric Content (%)	Outdoor Air Fiber + Fragment Polymeric Content (%)
FT-IR	15	4.8
	25 excluding cellulose	13 excluding cellulose
Raman	63	47

Supplemental Material

Microplastics Differ Between Indoor and Outdoor Air Masses: Insights From Multiple Microscopy Methodologies

Emily Gaston,[1,]* Mary Woo,[1] Clare Steele,[1] Suja Sukumaran,[2] Sean Anderson[3]

[1]California State University Channel Islands, Environmental Science and Resource Management Program, CA 93012 USA

[2]Thermo Fisher Scientific, San Jose, CA 95134 USA

[3]California State University Channel Islands, Environmental Science and Resource Management Program, PIRatE Lab, CA, 93012 USA

*Corresponding author email: Emily.Gaston@csuci.edu

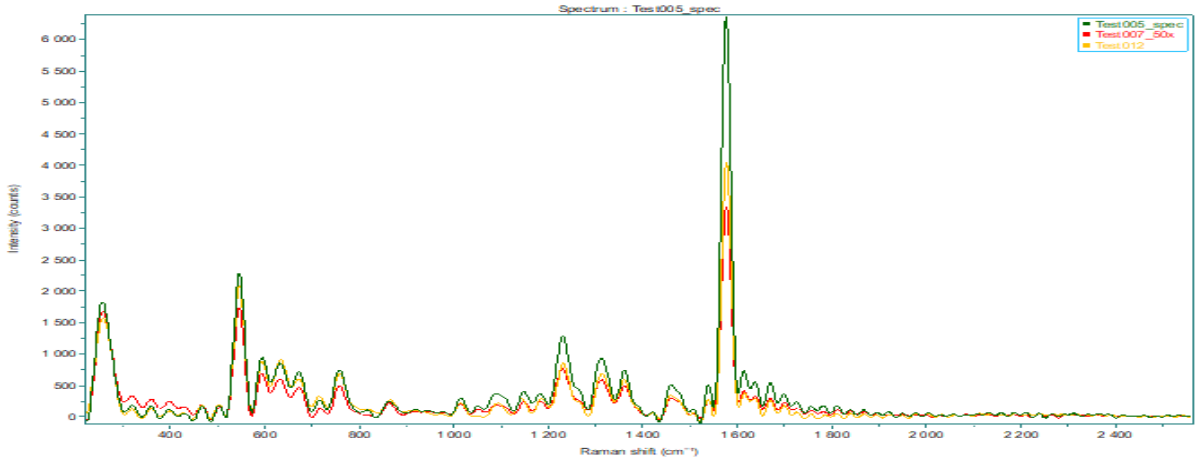

DOI: 10.1177/0003702820920652

Figure S1. Spectra of the same fiber on a glass slide, dry GF filter, and wet GF filter.

Table S2. List of chemical types, counts, and application identified as polymeric by μRaman.

Chemical Type	Counts (items)	Percent	Application
di-n-butyldichlorotin	15	42%	heat stabilizer in PVC
Valfor 100 Zeolite	4	11%	heat stabilizer in PVC
polyphosphoric acid	4	11%	additive to polymeric asphalt
1,2,3 triazole	4	11%	photostablizer in polymers
copper phthalocyanine	1	3%	common dye in polymers
PVC	2	6%	widespread consumer use in plastic
PE	2	6%	widespread consumer use in plastic
Resin	2	6%	widespread consumer use in plastic
PS	1	3%	widespread consumer use in plastic
ABS	1	3%	widespread consumer use in plastic
acrylic	1	3%	widespread consumer use in plastic
PC	1	3%	widespread consumer use in plastic

Table S1. DI water and microplastic counts.

DOI: 10.1177/0003702820920652

Water	Replicate	Date	Volume	Red Fibers	Orange Fibers	Yellow Fibers	Green Fibers	Blue Fibers	Purple Fibers	Brown Fibers	Black Fibers	Film	Fragments	Total fibers	Total plastics	Fiber richness
DI Water	1	3/13/19	1	0	0	0	0	2	1	0	0	2	0	5	5	2
DI Water	2	3/13/19	1	0	0	0	0	2	4	0	0	1	0	7	7	2
DI Water	3	3/13/19	1	0	0	0	0	1	1	0	0	1	0	3	3	2
DI Water	4	3/13/19	1	0	0	0	1	0	0	0	0	0	0	1	1	1
DI Water	5	3/13/19	1	0	0	0	0	3	1	0	0	1	0	5	5	2
DI Water	6	3/13/19	1	0	0	0	0	0	1	0	0	0	0	1	1	1
DI Water	7	3/13/19	1	0	0	0	0	1	0	0	0	1	0	2	2	1
DI Water	8	3/15/19	1	0	0	0	0	4	2	0	0	0	0	6	6	2

DOI: 10.1177/0003702820920652

DI Water	9	3/15/19	1	1	0	0	0	3	1	0	0	0	2	5	7	3
DI Water	10	3/15/19	1	0	0	0	0	0	0	0	0	0	1	0	1	0
DI Water	11	3/15/19	1	0	0	0	0	2	1	0	0	0	0	3	3	2
DI Water	12	3/15/19	1	1	0	0	0	1	1	0	0	0	0	3	3	3
DI Water	13	3/15/19	1	0	0	0	0	1	2	0	0	1	0	4	4	2
DI Water	14	3/15/19	1	0	0	0	0	0	0	0	0	0	0	0	0	0
DI Water	15	3/15/19	1	0	0	0	0	0	3	0	0	0	0	3	3	1
DI Water	16	3/15/19	1	0	0	0	0	0	0	0	0	2	0	2	2	0
DI Water	17	3/26/19	1	0	0	2	0	3	6	0	0	1	0	12	12	3

DOI: 10.1177/0003702820920652

DI Water	18	3/26/19	1	0	0	0	0	2	3	0	0	1	0	6	6	2
DI Water	19	3/26/19	1	0	0	0	0	0	3	0	0	1	0	4	4	1
DI Water	20	3/26/19	1	0	0	0	0	2	2	0	0	1	0	5	5	2
DI Water	21	3/26/19	1	0	0	1	0	2	2	0	0	3	0	8	8	3
DI Water	22	3/26/19	1	0	0	0	0	0	1	0	0	2	0	3	3	1
DI Water	23	3/26/19	1	0	0	0	0	1	0	0	0	1	0	2	2	1
DI Water	24	3/26/19	1	0	0	0	0	2	0	0	0	0	0	2	2	1
DI Water	25	3/26/19	1	0	0	0	0	0	0	0	0	0	0	0	0	0
DI Water	26	3/26/19	1	0	0	0	0	2	1	0	0	0	0	3	3	2

DOI: 10.1177/0003702820920652

DI Water	27	3/26/19	1	0	0	0	0	1	1	0	0	1	0	3	3	2
DI Water	28	3/26/19	1	0	0	0	0	3	0	0	0	0	0	3	3	1
DI Water	29	3/27/19	1	0	0	0	0	1	0	0	0	1	1	2	3	1
DI Water	30	3/27/19	1	0	0	0	0	0	1	0	0	2	0	3	3	1
DI Water	31	3/27/19	1	0	0	0	0	2	1	0	0	1	0	4	4	2
DI Water	32	3/27/19	1	0	0	0	0	1	0	0	0	0	0	1	1	1
DI Water	33	3/27/19	1	0	0	0	0	4	0	0	0	0	0	4	4	1
DI Water	34	3/27/19	1	0	0	0	0	1	1	0	0	0	0	2	2	2
DI Water	35	3/27/19	1	0	0	0	0	1	3	0	0	0	0	4	4	2

DOI: 10.1177/0003702820920652

DI Water	36	3/27/19	1	0	0	0	0	1	3	0	0	0	0	4	4	2
DI Water	37	3/27/19	1	0	0	0	0	1	0	0	0	0	0	1	1	1
DI Water	38	3/27/19	1	0	0	0	0	0	1	0	0	0	0	1	1	1
DI Water	39	3/27/19	1	0	0	0	0	0	1	0	0	0	0	1	1	1
DI Water	40	3/27/19	1	0	0	0	0	1	0	0	0	0	1	1	2	1
DI Water	Total:			2	0	3	1	51	48	0	0	24	5	129	134	